

**Nanohertz Frequency Determination
for the Gravity Probe B HF SQUID Signal**

M. Salomon* and J.W. Conklin†

*Department of Aeronautics & Astronautics,
Stanford University,
Durand Building, 496 Lomita Mall,
Stanford, CA 94305-4035*

J. Kozaczuk‡

*Department of Physics, University of California Santa Cruz,
211 Interdisciplinary Sciences Building,
1156 High Street Santa Cruz, CA 95064*

J.E. Berberian§ and D.I. Santiago¶

*Berberian & Company, LLC,
3865 Wilson Blvd Ste 520,
Arlington, VA 22203-1764*

G.M. Keiser,** A.S. Silbergleit,†† and P. Worden‡‡

*Hansen Experimental Physics Laboratory,
Stanford University, 452 Lomita Mall,
Stanford, CA 94305-4085*

(Dated: January 23, 2022)

Abstract

In this paper, we present a method to measure the frequency and the frequency change rate of a digital signal. This method consists of three consecutive algorithms: frequency interpolation, phase differencing, and a third algorithm specifically designed and tested by the authors. The succession of these three algorithms allowed a 5 parts in 10^{10} resolution in frequency determination. The algorithm developed by the authors can be applied to a sampled scalar signal such that a model linking the harmonics of its main frequency to the underlying physical phenomenon is available. This method was developed in the framework of the Gravity Probe B (GP-B) mission. It was applied to the High Frequency (HF) component of GP-B's Superconducting QUantum Interference Device (SQUID) signal, whose main frequency f_z is close to the spin frequency of the gyroscopes used in the experiment. A 30 nHz resolution in signal frequency and a 0.1 pHz/sec resolution in its decay rate were achieved out of a succession of 1.86 second-long stretches of signal sampled at 2200 Hz. This paper describes the underlying theory of the frequency measurement method as well as its application to GP-B 's HF science signal.

PACS numbers: 02.70.Rr, 06.30.Ft, 07.05.Kf

*Electronic address: michael.salomon@stanfordalumni.org

†Electronic address: johnwc@stanford.edu

‡Electronic address: jkozaczu@ucsc.edu

§Electronic address: berberian@alum.mit.edu

¶Electronic address: davitivan@gmail.com

**Electronic address: mackeiser@gmail.com

††Electronic address: gleit@stanford.edu

‡‡Electronic address: pworden@stanford.edu

I. BACKGROUND AND AVAILABLE SIGNAL

The GP-B experiment aims at testing in Earth orbit two predictions of Einstein's general relativity using precision gyroscopes. This idea was independently proposed by Pugh [1] and Schiff [2] [3] in 1960. Both of these authors pointed out that according to the general theory of relativity, the angular momentum axis of a gyroscope in orbit about the Earth will precess about a direction normal to the orbital plane due to the gravitational interaction of the spinning gyroscope with its orbital motion, and simultaneously about the direction of the Earth's rotation axis due to the interaction of the spinning gyroscope with the angular momentum of the Earth. The first effect is known as the geodetic effect, and the second is known as the frame-dragging effect. On a 640 km polar orbit, the gyroscope drift rate due to the orbital motion about the Earth is 6.6 arcsec/yr ($32 \mu\text{rad}/\text{yr}$), while the orbital average drift rate due to the Earth's angular momentum is 0.041 arcsec/yr ($0.20 \mu\text{rad}/\text{yr}$).

GP-B uses four gyroscopes spinning in a quasi torque-free environment and placed inside a drag-free satellite. The orientation of the gyroscopes is known thanks to an on-board telescope pointing towards a distant guide star, whose orientation with respect to an extragalactic source is known. Furthermore, the satellite rolls about the telescope axis. As the orientation of the satellite with respect to an inertial reference frame is nonetheless known, reference frames linked to the satellite are qualified as inertial throughout this paper. GP-B's scientific goal can be fulfilled by measuring the orientation of the gyroscope's spin axis with respect to the satellite.

The gyroscopes are superconductive, which allows tracking of the orientation of their angular velocity vectors. Indeed, a spinning, superconducting body creates a magnetic dipole parallel to its spin axis, the London moment [4] [5]. This magnetic dipole is then an excellent indicator of the direction of the instantaneous spin axis. Since the gyroscopes are almost perfectly spherical and uniform ($\Delta I \leq 10^{-6}$), the spin axis direction is a very good indicator of the direction of the angular momentum.

Low-noise Superconducting QUantum Interference Device (SQUID) magnetometers are thus used to measure the magnetic flux through a pick-up loop placed around each gyroscope created by the London moment plus a contribution due to a magnetic field trapped in the rotor. The SQUID signal is proportional to the magnetic flux through the pick-up loop. The SQUID output is an analog signal which, on board the satellite, is split into a low frequency

(LF) channel—which contains the London moment contribution—and a high frequency (HF) channel. Both HF and LF channels pass through a 780 Hz low pass analog filter. The LF channels then passes through an additional 4 Hz analog low pass filter and an additional gain stage. In this paper, we are only concerned about the HF channel, which is sampled at 2200 Hz and digitized with a 16 bit ADC with a range of ± 10 V. This ADC provides a resolution higher than the signal-to-noise ratio which is $\sim 10^5$ near the gyroscope spin frequency. We refer to this digitized high resolution signal as the "HF SQUID signal".

When each gyroscope transitioned below its critical temperature, the flux due to the residual magnetic field surrounding it before the transition was trapped on its surface, forming a large number of small magnetic sources. These sources are called fluxons, and can be pictured as rigidly linked to the surface of the body, as shown for instance in [9]. A consequence is that the fluxons exactly follow the motion of the body and create modulations, on the order of a few volts, at a frequency close to the spin frequency of the gyroscope: these modulations constitute the HF signal.

The HF SQUID signal is sent intermittently in the form of 1.86 second long stretches that we refer to as "snapshots". Each snapshot contains 4096 points. We also have access to this signal in the form of Fast Fourier Transforms (FFTs) performed at regular intervals on the SQUID signal by the on-board CPU. The FFT is applied every 10 seconds to sets of 4096 points of raw data, and a compacted form of its output is sent to the ground.

An on-board FFT algorithm is applied to 1.86 second-long stretches of HF SQUID signal and can thus resolve frequencies $1/1.86 \text{ sec} = 0.54 \text{ Hz}$ apart. This frequency resolution, called a 'bin', is poor: the FFT data is thus further processed. This additional processing is performed on the ground, and requires computing the FFT at a few frequencies. The value of the FFT at the first five harmonics of the signal frequency and the one corresponding to the 110 Hz calibration signal are thus telemetered. In addition, the value of the FFT at the two bins adjacent to each one of these six frequencies are also sent down, as well as the zero-frequency term. For each 1.86 second-long data stretch, the on-board FFT algorithm thus provides 19 data points. Since the high frequency data is sampled at 2200 Hz, the initial data stretch contains 4096 points and so does its FFT, so transmitting 19 data points is a dramatic reduction in bandwidth.

Additionally, raw snapshots of the SQUID signal are also sent down on an irregular but frequent basis. These snapshots also consist of 1.86 second-long data stretches sampled at

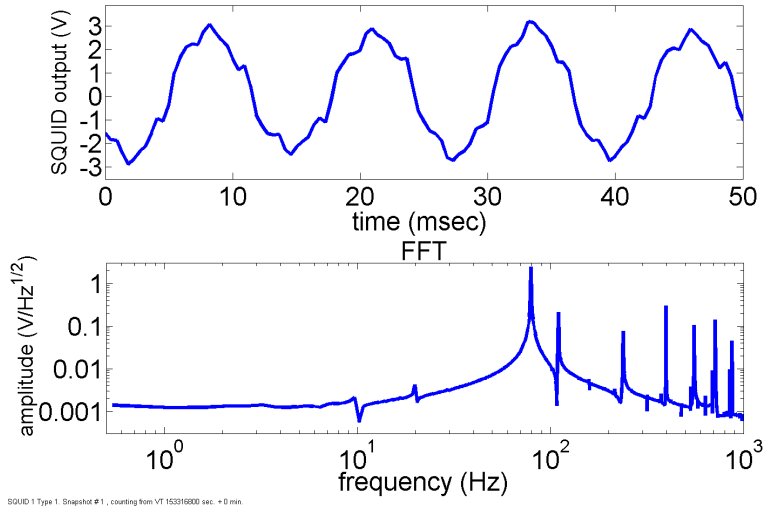


FIG. 1: (Color online) Snapshot (time-series and spectrum) for Gyroscope 1, taken November 10, 2004

2200 Hz. An example of the time history of a portion a snapshot is provided in the upper pane Figure 1, while the FFT of the entire shapshot is shown in the lower pane.

In this paper, we describe the method that was used to determine the frequency of this HF signal, and therefore the rotor spin speed, with a resolution better than 30 nHz. This was critical for the GP-B data analysis because it allowed the time-varying readout scale factor to be determined to 1 part in 10^4 , the orientation of the spin axis with respect to the spacecraft to be determined to ~ 3 marcsec in 1 orbit, and the gyroscopes' relativistic drift rates to be determined to 20 marcsec/yr [6]. The time-varying scale factor is caused by the trapped flux contribution to the magnetic flux through the pick-up loop, which varies at the rotor spin \pm spacecraft roll frequency, the rotor polhode frequency and at low frequency. With an accurate estimate of the rotor polhode and the estimate of the rotor spin speed to 30 nHz (discussed here) the body-fixed orientation of the gyroscope rotor with respect to the spacecraft was determined with an accuracy of ~ 1 deg throughout the entire science mission, lasting 1 year. This information was necessary to determine the distribution of trapped flux on the surface of the rotor and the time varying readout scale factor [7].

Before delving into the 3 successive frequency estimation algorithms, we introduce notations specific to the GP-B experiment in order to explain the relationship between the gyroscope motion and the SQUID signal. We then describe how frequency interpolation

and phase differencing, a time-domain technique, were applied to the FFT data to achieve a $5 \mu\text{Hz}$ frequency resolution. We then show that this result was checked using the snapshot data. Variations of these first two techniques are known and their accuracy in determining monotone signals in the presence of Gaussian white noise and simple systematic effects have been studied [8]. Finally, we show how the snapshot data and the result of the phase differencing were used to run the algorithm developed by the authors which allowed a 5 parts in 10^{10} accuracy in frequency determination.

II. GYROSCOPE MOTION AND HF SQUID SIGNAL FREQUENCY

As the fluxons attached to the gyroscope move with it, HF modulations are created in the SQUID signal. The fluxons create a body-fixed distribution of potential: a model for this distribution can thus be written in body-fixed frame, for instance using a spherical harmonics expansion [10, 12]. The SQUID measurement however takes place in the satellite frame - which, as explained above, is considered inertial. Therefore, if the appropriate set of Euler rotations is applied to rotate the body-fixed frame into the inertial frame, it is possible to express the HF SQUID signal as a function of the coefficients of the model of the magnetic potential distribution.

The vectors \vec{I}_1 , \vec{I}_2 and \vec{I}_3 are the principal inertia axes of the gyroscope and define an orthonormal body-fixed reference frame. We call $(\vec{x}_1, \vec{y}_1, \vec{z}_1)$ an orthonormal inertial reference frame such that \vec{z}_1 is aligned with the angular momentum \vec{L} of the gyroscope. The angular momentum is inertially fixed as the gyroscopes are in torque-free motion. These notations are shown in figure 2.

The first Euler rotation from $(\vec{I}_1, \vec{I}_2, \vec{I}_3)$ to $(\vec{x}_1, \vec{y}_1, \vec{z}_1)$ is an azimuthal rotation by an angle ϕ_p . This rotation transforms $(\vec{I}_1, \vec{I}_2, \vec{I}_3)$ into a reference frame $\vec{x}'\vec{y}'\vec{z}'$ whose \vec{z}' axis is aligned with \vec{I}_3 . A polar rotation by an angle γ is then applied: the new reference frame $\vec{x}''\vec{y}''\vec{z}''$ is such that its third axis \vec{z}'' is aligned with the angular momentum. The third Euler angle ϕ_s measures the angle by which the gyroscope has spun about \vec{L} since a fixed time origin: a rotation of angle $-\phi_s$ about \vec{L} is thus also needed to obtain the inertial reference frame $(\vec{x}_1, \vec{y}_1, \vec{z}_1)$.

Consequently, the frequency at which any fluxon passes through the pick up loop is $\dot{\phi}_s/2\pi + f_p$, where f_p is the polhode frequency, such that $f_p \sim \dot{\phi}_p/2\pi$. As the modulations

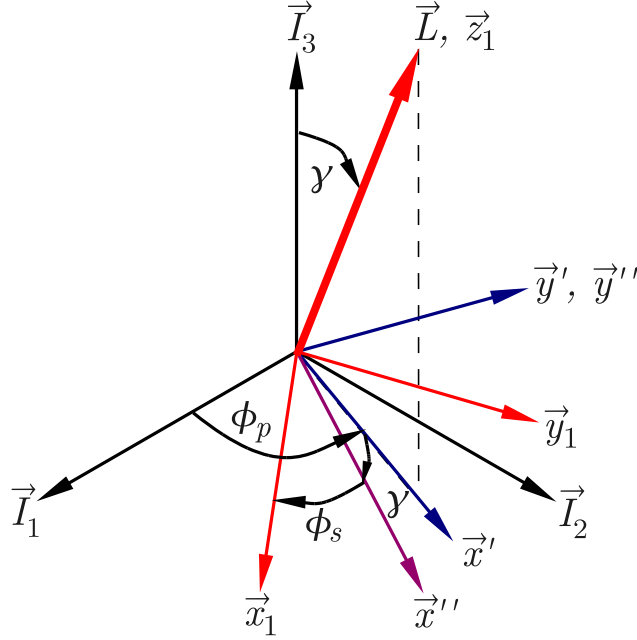


FIG. 2: (Color online) Rotations from body fixed frame $(\vec{I}_1, \vec{I}_2, \vec{I}_3)$ to inertial frame $(\vec{x}_1, \vec{y}_1, \vec{z}_1)$

in the HF SQUID signal are due to the motion of the fluxons with respect to the pick-up loop, the frequency f_z of this signal is thus given by:

$$f_z = \frac{1}{2\pi} \dot{\phi}_s + f_p. \quad (1)$$

An expression for $\dot{\phi}_s$ can be obtained from [13], formulas 89.4 and 90.4:

$$\dot{\phi}_s = \frac{L}{I_3} \left[1 + \frac{I_3 - I_1}{I_1} \frac{1}{1 + \alpha^2 \text{sn}^2(\tau, k^2)} \right], \quad (2)$$

where the characteristic, α , and the elliptic modulus, k , only depend on the moments of inertia I_1 , I_2 and I_3 , the rescaled time, τ , depends on the three moments of inertia and the angular momentum, L (see [10]) and sn is the Jacobi elliptic integral referred to as "sinus amplitude" and defined by:

$$\text{sn}(\tau, k) = x \quad \text{when} \quad \tau = \int_0^x \frac{ds}{\sqrt{(1-s^2)(1-k^2s^2)}}.$$

The first term in Eq. (2) is the larger by a factor of 10^6 , and the second term is a modulation at twice the polhode frequency. The three Euler rotations are summarized in the definition

of the spin axis $\vec{\omega}$:

$$\vec{\omega} = \dot{\phi}_p \vec{I}_3 + \dot{\gamma} \vec{y}' - \dot{\phi}_s \vec{z}''.$$

The spin frequency f_s is thus

$$(2\pi f_s)^2 = \dot{\phi}_p^2 + \dot{\phi}_s^2 + \dot{\gamma}^2 + 2\dot{\phi}_s \dot{\phi}_p \cos \gamma. \quad (3)$$

As $\dot{\phi}_p$ and $\dot{\gamma}$ can be as large as f_p which is on the order of 0.1 mHz on all gyroscopes [10], $\dot{\phi}_s$ lies within 0.1 mHz of the spin frequency f_s and is thus on the order of 100 Hz. The HF SQUID signal frequency f_z is thus close to the spin frequency f_s .

The first two steps of the frequency determination method presented in this paper are applied to the HF SQUID signal in order to determine f_z . The third step of the frequency determination method presented in this paper thus aims at determining $\dot{\phi}_s$ with a 20 nHz resolution. In [10], a procedure is given to measure the polhode frequency f_p with a 10 nHz accuracy. Note that this represents an accuracy of 1 part in 10^4 as the polhode frequency is on the order of 0.1 mHz. Therefore, from (1), an absolute accuracy better than 30 nHz in the the determination of the frequency f_z of the HF SQUID signal can be achieved. In relative terms, the claimed accuracy of the frequency f_z determination is thus on the order of 5 part in 10^{10} .

III. MILLIHERTZ LEVEL SIGNAL FREQUENCY DETERMINATION THROUGH FREQUENCY INTERPOLATION

By interpolating the FFT data, it is possible to go beyond the 0.54 Hz frequency resolution and to determine the frequency with a 1 mHz precision. This method is well known and has been used for several decades [11]. It consists of approximating the signal by a pure sine around its main frequency, and finding the frequency of such a sine if it had the same amplitude diagram as the FFT of the signal. We now give a mathematical description of this method.

As the interpolation is applied to the FFT data which is itself computed using short stretches of SQUID signal, we neglect the polhode harmonics in this description. We show, without loss of generality, how frequency interpolation is implemented for a single frequency signal.

Let $z_{\text{HF}}(t)$ be our signal, so that

$$z_{\text{HF}}(t) = A_s \cos(2\pi f_z t + \delta\phi(t)).$$

Its discrete Fourier transform is:

$$F(f) = \frac{A_s}{2} e^{i\delta\phi} e^{-i2\pi(f-f_z)\Delta t \frac{N-1}{2}} \left[\frac{\sin[2\pi(f-f_z)\Delta t N/2]}{\sin[2\pi(f-f_z)\Delta t/2]} \right] + \frac{A_s}{2} e^{-i\delta\phi} e^{-i2\pi(f+f_z)\Delta t \frac{N-1}{2}} \left[\frac{\sin[2\pi(f+f_z)\Delta t N/2]}{\sin[2\pi(f+f_z)\Delta t/2]} \right] \quad (4)$$

where: Δt is the time between two consecutive samples (1/2200 sec for a 2200 Hz sampling rate), $N = 4096$ is the number of points in the FFT, $N\Delta t$ is then the total snapshot duration, $f_d = 1/(N\Delta t)$ is the bin frequency, f is the frequency at which the FFT is computed, A_s is the signal amplitude and $\delta\phi$ is the phase shift.

Near the HF signal's frequency, $f \approx f_z$, so the first term in (4) is dominant and we neglect the second one. Since the FFT is discrete, we only obtain its values at multiples of the bin frequency f_d . Furthermore, as mentioned above, we have at our disposal the value of the FFT at the central bin and at the two adjacent bins. Let's define the integer n such that nf_d is the multiple of f_d closest to the signal frequency f_z . We note:

$$F_n = F(nf_d) \quad F_{n+1} = F[(n+1)f_d] \quad F_{n-1} = F[(n-1)f_d].$$

Then the quantity we use in the interpolation is:

$$F_n = \frac{A_s}{2} e^{i\delta\phi} e^{-i2\pi(nf_d-f_z)\Delta t \frac{N-1}{2}} \left[\frac{\sin[2\pi(nf_d-f_z)\Delta t N/2]}{\sin[2\pi(nf_d-f_z)\Delta t/2]} \right].$$

F_{n-1} and F_{n+1} are defined similarly. Let's also introduce the ratios:

$$R_{n+1} = \left| \frac{F_{n+1}}{F_n} \right| \quad R_{n-1} = \left| \frac{F_{n-1}}{F_n} \right|.$$

The values of those two ratios are obtained from measurements. We define the quantity x_n to be,

$$x_n = 2\pi(nf_d - f_z)N\Delta t/2. \quad (5)$$

Then, by performing a Taylor series expansion of F_m in the quantity x_m/N , where m takes values $n-1$, n , $n+1$, we obtain,

$$R_{n+1} = \left| \frac{x_n}{x_n + \pi} \right| + \mathcal{O}\left(\frac{x_n}{N}\right) \quad R_{n-1} = \left| \frac{x_n}{x_n - \pi} \right| + \mathcal{O}\left(\frac{x_n}{N}\right). \quad (6)$$

As implied by Eq. 5, the term (x_n/N) here is 10^{-3} at most, since near the main peak the signal frequency, f_z , is at worst one frequency bin away from nf_d . From these relations, we derive two formulas for the frequency f_z of the HF SQUID signal, depending on the sign of x_n . For $x_n > 0$:

$$f_z = nf_d + \frac{1}{N\Delta t} \frac{R_{n+1}}{R_{n+1} - 1} + \mathcal{O}(10^{-3}), \quad (7)$$

$$f_z = nf_d - \frac{1}{N\Delta t} \frac{R_{n-1}}{R_{n-1} + 1} + \mathcal{O}(10^{-3}). \quad (8)$$

Averaging the two formulas for f_z we and obtain:

$$f_z = nf_d + \frac{1}{2N\Delta t} \left[\frac{R_{n+1}}{R_{n+1} - 1} - \frac{R_{n-1}}{R_{n-1} + 1} \right] + \mathcal{O}(10^{-3}) \quad (9)$$

For $x_n < 0$:

$$f_z = nf_d + \frac{1}{N\Delta t} \frac{R_{n+1}}{R_{n+1} + 1} + \mathcal{O}(10^{-3}), \quad (10)$$

$$f_z = nf_d + \frac{1}{N\Delta t} \frac{R_{n-1}}{R_{n-1} - 1} + \mathcal{O}(10^{-3}). \quad (11)$$

Averaging these two formulas gives:

$$f_z = nf_d + \frac{1}{2N\Delta t} \left[\frac{R_{n+1}}{1 + R_{n+1}} + \frac{R_{n-1}}{R_{n-1} - 1} \right] + \mathcal{O}(10^{-3}) \quad (12)$$

Therefore, the frequency interpolation yields a determination of the HF signal's frequency f_z , whose error is $\mathcal{O}(x_n/N) \lesssim \pi/N$, or 10^{-3} Hz. Indeed, the frequency computed by this method typically showed a 100 μ Hz spread, as shown on figure 3.

The result derived in (12) was obtained for the simple case of a signal with only one harmonic. However, the HF signal contains many harmonics of its main frequency, and as explained in [10, 14], the odd harmonics have a significantly larger amplitude. The interpolation procedure is therefore separately applied to the fundamental frequency, f_z , as well as to the 3rd and 5th harmonics of the FFT data. The results from each of those 3 interpolations are then averaged in order to obtain a determination of the signal frequency f_z . Results for a 6-hour long data stretch for gyroscope 1 are shown in figure 3.

The formula (12) for the signal's frequency is valid when no window is applied. Applying windows to a signal consists of multiplying it by a carefully chosen function -for example, a sine square- so the frequency components away from the main frequency are attenuated

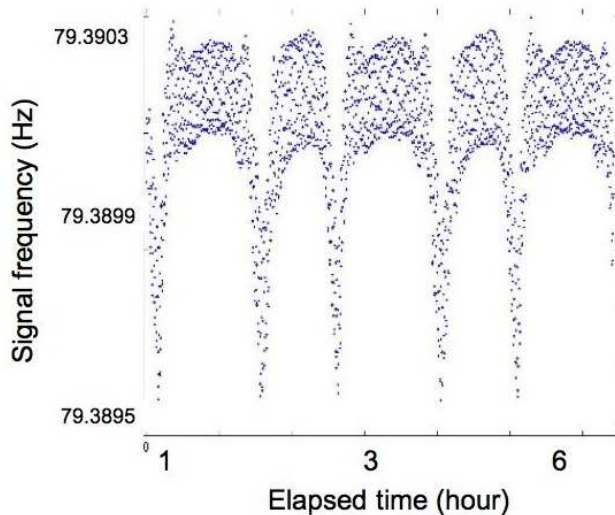


FIG. 3: (Color online) Frequency f_z from interpolation, gyroscope 1, Aug. 19 2004

[15, 16]. In the case of the windowed signal, the analytical expression of f_z is more complex but the principle of the derivation remains exactly the same.

IV. MICROHERTZ LEVEL SIGNAL FREQUENCY DETERMINATION THROUGH PHASE DIFFERENCING

The interpolation method relies on the use of the amplitude of each independent FFT and, in practice, yields a 1 mHz or better frequency resolution. We now present an additional method called phase differencing that uses the phase of the peak FFT bin, which is the one closest to the frequency of interest, at two different times. This method yields more than two additional orders of magnitude in frequency resolution. Phase differencing consists of using a precise measurement of the change in the phase of the FFT computed on two distinct 1.86 second-long data stretches. Knowing the time elapsed between the two data stretches, we can determine the signal frequency. However, to resolve the 2π ambiguity, an initial estimate of this frequency is necessary. Indeed, let ϕ_1 be the phase of the FFT obtained at time t_1 and ϕ_2 the phase of the FFT obtained at time t_2 . We can assume that the frequency f_z of the signal is constant if t_1 and t_2 are close (we indeed show later that the characteristic time of the decay in f_z is 7,000 - 25,700 years, depending on the gyroscope). We then have:

$$\phi_2 - \phi_1 = 2\pi f_z(t_2 - t_1) - 2\pi K, \quad (13)$$

where K is an integer such that $\phi_2 - \phi_1$ is between 0 and 2π . We then need to know the value of K in order to extract the frequency f_z from the previous equation. This requires knowing an estimate f_z^{est} of the signal frequency so that:

$$2\pi f_z^{est}(t_2 - t_1) - 2\pi K \in [0, 2\pi]. \quad (14)$$

The value of K then has to be chosen to ensure condition (14). In order for K to be known, f_z^{est} must lie within 1/10 Hz of the real value f since $(t_2 - t_1) = 10$ sec. This resolution is easily achieved by the interpolation algorithm. Furthermore, this 1/10 Hz requirement is more stringent than the 0.54 Hz precision of the FFT: the result of the interpolation is thus needed to carry out the phase differencing.

Then, once K is computed, equation (13) can trivially be solved for the signal frequency f_z . This new estimate has a very good precision. Indeed, the phase is known with a conservative error of 10 arcsec (5×10^{-5} rad), which at the gyroscope spin speed corresponds to a timing error of approximately 7×10^{-8} sec, which may be compared to the short-term on-board clock accuracy of approximately 10^{-8} sec. The main error term is thus the phase measurement, and for a $(t_2 - t_1) = 10$ sec interval, we obtain a precision better than 5 μ Hz. Figure 4 shows the extra resolution that can be achieved with phase differencing. It should be compared with figure 3, which only shows the output of the interpolation on the same data stretch.

The large modulations in f_z are at polhode frequency and are a systematic error in the estimation method. Indeed, we used a simple model for the HF signal z_{HF} which only takes into account the harmonics of f_z , whereas harmonics of the polhode frequency also contribute to the signal's spectrum. These frequencies then leak into our current measurement of f_z . The model introduced in the last section of this article takes into account all the frequency components of the HF signal, and yields an estimate of f_z free of large variations at polhode frequency.

As a conclusion, by interpolating each FFT and using phase differencing between FFTs, we can obtain an estimate of the signal frequency with an error of a few μ Hz. We have thus gained 5 orders of magnitude as compared to the FFT bin width of 0.54 Hz. Furthermore, this determination only relies on estimates of the FFT for a small number of frequencies

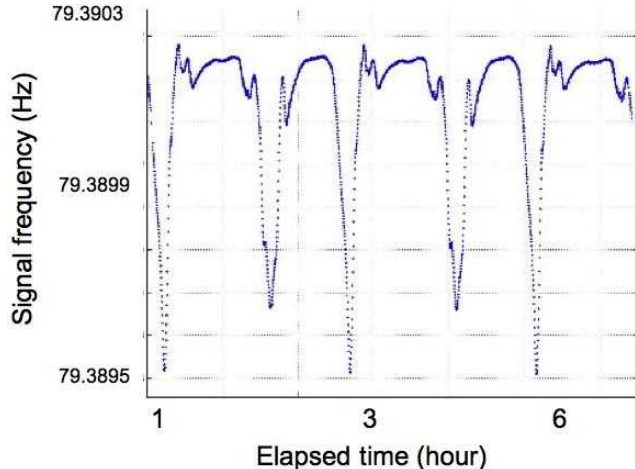


FIG. 4: (Color online) Frequency f_z from phase differencing, gyroscope 1, Aug. 19 2004

gyro	signal frequency f_z (Hz)
1	79.38715
2	61.81759
3	82.09202
4	64.85030

TABLE I: Typical values for signal frequency f_z obtained from phase differencing

being transmitted from the spacecraft. It then has the double advantage of requiring little bandwidth and using less on-board CPU time, since the interpolation and the phase differencing are carried out on the ground. Typical values for f_z obtained after phase differencing are given in table I. They have been measured on Feb. 6th 2005 at 07:39 GMT.

Figure 5 shows a linear decay of the frequency f_z for gyroscope 4 over four months. This decay was observed on all four gyroscopes. As the polhode frequency f_p increased slowly throughout the experiment, equation (1) implies that the decay in frequency can be attributed to a decay in $\dot{\phi}_s$.

The FFT is taken on-board every 10 seconds for approximately 40% of each orbit, a period called Guide Star Invalid (GSI). During the rest of the orbit, the Guide Star Valid (GSV) period, the on-board FFT algorithm is turned off in order to allow the CPU capacity

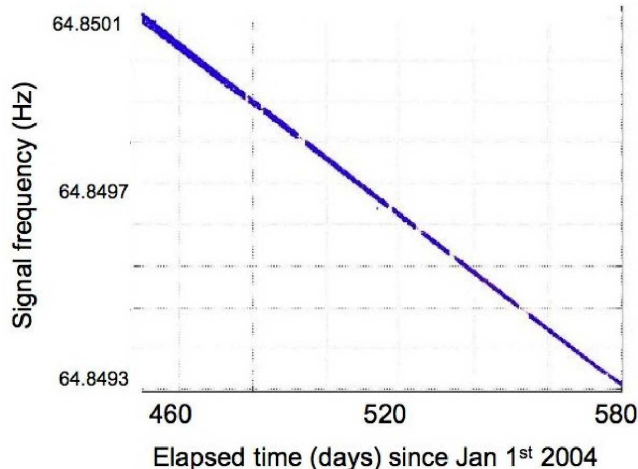


FIG. 5: (Color online) HF signal frequency f_z on gyroscope 4 over 4 months

to be used to track the guide star: we then have about 4000 frequency measurements per day with a 10-second spacing, each one with a $5 \mu\text{Hz}$ standard deviation. A covariance analysis yields a 0.1 nHz/sec uncertainty on the value of the signal frequency decay rate using 24 hours worth of data (assuming 16 GSI periods per day, each lasting 40 minutes and containing 240 samples, and that for each GSI period a frequency offset must be estimated together with the decay rate). An averaging time of 24 hours is chosen because there are sometimes large gaps in the FFT data, ranging from a few hours to a few days, that occurred at roughly 1-2 day intervals that preclude longer averaging times. These gaps are related to details of the spacecraft operations and, on rare occasions, to spacecraft anomalies.

Typical values for the frequency decay rate and the characteristic time of the decay are given in table II.

V. VERIFICATION USING SNAPSHOT DATA

The results obtained so far are derived from the analysis of the FFT data. To increase the level of confidence in these results, they have been checked by an independent verification using the snapshot data. These data are more voluminous, hence much richer, than the FFT data: a snapshot comprises 4096 points, whereas an FFT compacts it into 19 points. Typically, snapshots are transmitted about every 40 seconds during approximately an hour,

gyro	frequency decay rate (nHz/sec)	characteristic time of decay (years)
1	0.16	15,800
2	0.14	13,400
3	0.36	7,000
4	0.08	25,700

TABLE II: Typical decay rate and characteristic time for the frequency f_z of the HF signal

separated by gaps ranging from an hour to up to two days.

A two-step algorithm similar to the procedure followed in the FFT analysis was implemented in order to determine the signal frequency from the snapshot data. First, a Fast Fourier Transform of each snapshot was performed and interpolated in order to produce an initial estimate of the spin frequency. A two-point interpolation algorithm was used (instead of three-point) to simplify the coding. A least-squares fit of each snapshot to a sum of up to 51 harmonics of the frequency obtained from the interpolation was then performed.

Secondly, a nonlinear fit to the snapshot data for the signal frequency, f_z , and the amplitudes of the sine and cosine components of $2\pi f_z t$ and its harmonics (up to the 51st) was performed using the *NonLinearRegress* routine available in Mathematica. The initial conditions were, for f_z , the value obtained after the interpolation and, for the harmonics coefficients, the output of the linear fit.

This two-step analysis yielded an independent estimation of the signal frequency as well as a large number of harmonics coefficients using a data set and a method which was different from those used in the FFT analysis.

Figure 6 compares f_z determined from the FFT and snapshot data on gyroscope 4 for February 7th 2005. Note that, like for the FFT data, the estimation of f_z obtained from the snapshot data shows variations at the polhode frequency. This is expected as the model for the signal used in this determination also neglects the harmonics of polhode. These results are typical and have been observed on all the gyroscopes throughout the mission. The signal's frequency obtained from the snapshots is typically noisier than the one obtained from the FFT (the spread is on the order of 30 μ Hz). The higher level of noise is likely due

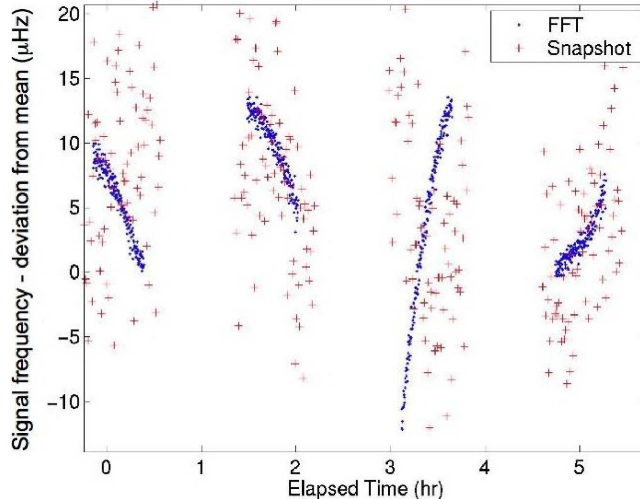


FIG. 6: (Color online) f_z obtained from FFT and snapshots, gyroscope 4, Feb. 7 2005

to the on-board analog-to-digital converter, which exhibited noise at all multiples of 10 Hz. Nevertheless, both time histories coincide strikingly despite the difference in data sets and in algorithms, which increases our confidence in the measurement.

Since more information is contained in the snapshot data, including harmonics higher than the 5th, it was used as a reference for the remainder of the analyses presented in this paper. The analog-to-digital converter noise is later estimated and subtracted from the snapshot data to remove its effects. A more detailed discussion of the justification for this choice can be found in [10]. The last step of the method indeed dramatically increases the signal's frequency resolution, which fully offsets the poorer quality of the determination obtained from the snapshots.

VI. NANOHERTZ LEVEL SIGNAL FREQUENCY DETERMINATION

A. Overview

The interpolation and phase differencing methods allowed a determination of the signal frequency f_z with a microhertz level accuracy. As the error in the determination of f_p is 10 nHz, formula (1) indicates that a better resolution in f_z can be achieved if $\dot{\phi}_s$ is measured accurately.

In section IV of this paper, it is shown that the linear decay in the measured frequency

f_z is due to a decay in $\dot{\phi}_s$. The expression given in (2) for $\dot{\phi}_s$ shows that the decaying term is necessarily the angular momentum L . We can then write:

$$\dot{\phi}_s = 2\pi(C_1 + C_2(t - t_0)) \left[1 + \frac{I_3 - I_1}{I_1} \frac{1}{1 + \alpha^2 s n^2(\tau, k^2)} \right], \quad (15)$$

where t_0 is a chosen time origin.

An accurate determination of the coefficients C_1 and C_2 is thus necessary to estimate $\dot{\phi}_s$. This last section describes how this estimation was carried out. The underlying principle is to expand the HF SQUID signal in harmonics of ϕ_s . A model for the complex amplitude $H_n(t)$ of the n^{th} harmonic of ϕ_s has been derived in [12] and is given in its compact form in equation (17): the values \hat{C}_1 and \hat{C}_2 yielding the time history for $\phi_s(t)$ such that the measured harmonics $H_n(t)$ are best accounted for by the model are taken as the best estimates of C_1 and C_2 .

Once C_1 and C_2 are known, the value of $\dot{\phi}_s$ can be computed from (15), and the signal's frequency f_z can be obtained from (1).

B. A cost function to estimate ϕ_s

Reference [12] gives an expansion of the HF SQUID signal z_{HF} in harmonics of ϕ_s :

$$z_{\text{HF}}(t) = \sum_{n=-\infty, n \neq 0}^{\infty} H_n(t) e^{-in(\phi_s(t))}, \quad (16)$$

A model for $H_n(t)$ with n odd can be derived using a similar procedure to that used in [12], and this has been done in [10, 14]. This model states that $H_n(t)$ depends on time only through the angles $\phi_p(t)$ and $\gamma(t)$, determined in [10], so that:

$$H_n(t) = H_n(\phi_p(t), \gamma(t)).$$

This model is furthermore linear in the coefficients of the expansion of the magnetic potential in the body-fixed frame. In other words, $H_n(\phi_p(t), \gamma(t))$ is linear in a state vector \vec{A} whose coefficients are constant as they only depend on the body-fixed magnetic potential distribution. We call $M_n(\phi_p(t), \gamma(t))$ the observability matrix for this linear model. Its expression is given in [10]. We can thus write:

$$H_n(\phi_p(t), \gamma(t)) = M_n(\phi_p(t), \gamma(t)) \vec{A}. \quad (17)$$

Therefore, if the Euler angle $\phi_s(t)$ is known accurately, $H_n(t)$ is known from (16), and by running a linear least squares algorithm, we can estimate the vector \vec{A} that minimizes the residuals J_1 where:

$$J_1 = \min_{\vec{A}} \left\| H_n(t) - M_n(\gamma(t), \phi_p(t)) \vec{A} \right\|. \quad (18)$$

However, errors in the estimation of C_1 and C_2 lead to an approximate value $\phi_s^{app}(t)$ for the third Euler angle. The coefficient $H_n^{app}(t)$ obtained from the expansion (16) of the HF signal in harmonics of $\phi_s^{app}(t)$ is therefore also approximate. Consequently, the model (17) does not apply exactly: the vector \vec{A}^{app} that solves the least squares problem (17) with the approximate value $H_n^{app}(t)$ for $H_n(t)$ yields a minimum norm J_1^{app} of the residuals which is larger than the value J_1 defined in (18).

Therefore, the best estimate $\hat{\phi}_s$ of the third Euler angle is the one that yields the smallest value for the residual J_1^{app} . In other words, $\hat{\phi}_s$ minimizes the functional J defined by

$$J[\phi_s] = \min_{\vec{A}} \left\| H_n[\phi_s](t) - M_n(t) \vec{A} \right\|. \quad (19)$$

The notation $J[\phi_s]$ means that the argument of the functional J is the function ϕ_s .

In reference [10], an expression for ϕ_s is given based on the integration of the expression (15) for $\dot{\phi}_s$:

$$\begin{aligned} \phi_s(t) &= \phi_{s_0} + 2\pi C_1 [(t - t_0) + \Pi_1(t, t_0, I_1, I_2, I_3, f_p)] \\ &\quad - 2\pi C_2 \left[\frac{1}{2}(t - t_0)^2 + \Pi_2(t, t_0, I_1, I_2, I_3, f_p) \right]. \end{aligned} \quad (20)$$

In this expression, ϕ_{s_0} is ϕ_s at the time origin t_0 . The terms Π_1 and Π_2 are integrals of the Jacobi elliptic function sn and depend only on the moments of inertia and the polhode frequency. The function ϕ_s is thus fully determined by three variables: ϕ_{s_0} , C_1 and C_2 .

Using equation (20), we see however that the initial value ϕ_{s_0} is just a constant shift to the angle $\phi_s(t)$. From the expansion (16), a constant shift in $\phi_s(t)$ yields a constant phase shift $e^{in\phi_{s_0}}$ in $H_n[\phi_s]$. In the expression (19), we can factor out this constant phase shift, so that the term \vec{A} becomes $\vec{A}e^{-in\phi_{s_0}}$. And since $J[\phi_s]$ is a minimum over all values of \vec{A} , its value is then independent of ϕ_{s_0} . Consequently, the best estimates of C_1 and C_2 minimize $J[\phi_s]$.

In other words, the estimation of C_1 and C_2 is a minimization problem of a function J_2 of two variables:

$$J_2(C_1, C_2) = \min_{\vec{A}} \left\| H_n(C_1, C_2, t) - M_n(\gamma(t), \phi_p(t)) \vec{A} \right\|. \quad (21)$$

We have thus constructed a cost function J_2 which can be minimized in order to estimate the two coefficients C_1 and C_2 .

This frequency determination method is general. Indeed, it only supposes that a model for the harmonics of the signal's frequency is available: the frequency yielding the harmonics best fit by the model is then the best estimate of the signal's frequency.

Note that in the specific case of the GP-B gyroscopes, the modeled quantities are not exactly the harmonics of the signal's frequency f_z of the signal but rather of $\dot{\phi}_s = 2\pi(f_z - f_p)$, where f_p is known accurately.

C. Implementation

We now introduce the algorithm developed by the authors to estimate C_1 and C_2 .

A nonlinear minimization routine based on a modification of the Nelder-Mead (NM) simplex [17], used in Matlab's *fnimsearch.m* function, was implemented. A simplex is a set of $n + 1$ points in an n -dimensional space such that the points are not degenerate. In 2-space the simplex is a triangle. A detailed account of how this algorithm works can be found in [14]. This nonlinear simplex routine was chosen because of its high accuracy for non-smooth objective functions compared with gradient or Gauss-Newton methods, implemented in Matlab's *lsqnonlin.m* function for example. The Nelder Mead simplex is a nonlinear minimization algorithm and as such requires the input of initial conditions. Since we know *a priori* the region of possible values for C_1 and C_2 , we utilize a NM simplex method that is modified to include a constraint on the search domain. From equation (15), we find that, for the GP-B gyroscopes:

$$\dot{\phi}_s(t_0) = 2\pi C_1(1 + \mathcal{O}(10^{-6}))$$

And since:

$$\dot{\phi}_s = 2\pi(f_z - f_p)$$

we find:

$$C_1 = (f_z(t_0) - f_p(t_0))(1 + \mathcal{O}(10^{-6}))$$

Using the measurement of f_z obtained previously, we thus have an initial condition for C_1 as well as a search interval whose width is on the order of 100 μHz .

Similarly, we use the measurement of the decay in f_z to find an initial condition and a search interval for C_2 . As $|df_p/dt|$ can be as large as $1/10 df_z/dt$, the relative size of the search interval is larger than for the coefficient C_1 : we opted for a search interval whose size is 25% of the measured decay rate of f_z .

Using these two initial conditions and search intervals, we define a search region in the (C_1, C_2) plane. The NM simplex algorithm will then search for the values of C_1 and C_2 within this region that minimize the cost function J_2 .

The NM algorithm is implemented in Matlab's built-in *fminsearch.m* routine. The algorithm first evaluates the cost function J_2 on a set of three points A , B and C , called a simplex, within the search region. The Matlab algorithm finds on which vertex A of the simplex the function has the maximum value. Let B and C be the other two vertices of the simplex and H the center of segment BC . The algorithm evaluates the function at a point A' such that AA' is orthogonal to BC and $AA' = \delta AH$ with $\delta = 3$. (see figure 7). This procedure is called an 'expansion'. Indeed, the simplex $A'BC$ has a bigger area than ABC . If the cost function J_2 has a lower value in A' than in A , the algorithm is searching in the right direction in the (C_1, C_2) plane, and the procedure repeats, now starting from A' . If the function has a higher value in A' than in A , the expansion did not decrease the value of the function and should then not be pursued. The cost function is then evaluated at a new point A'' inside the ABC simplex (see figure 8), such that $AH = \rho HA''$, where $\rho = 2$, and the procedure repeats. Matlab's algorithm stops when the dimension of the simplex, that is the length of its longest side, is lower than the specified tolerance.

There are two main limitations in the available Matlab routine. First, only one tolerance can be specified. This is in our case a real issue as both the absolute and relative tolerance on C_1 and C_2 differ by many orders of magnitude. Furthermore, the algorithm does not provide any way to decrease the likelihood of honing in on a local minimum.

Matlab's *fminsearch.m* routine was thus modified to address these two issues. First, a simple but crucial change was brought to *fminsearch.m* so that the termination tolerances on the two dimensions were allowed to differ: the modified NM algorithm terminates only when the length of the simplex along both the C_1 and C_2 dimensions are smaller than values yielding the required precision in $\dot{\phi}_s$: these numbers are referred to as "termination tolerances".

After examining several algorithms for decreasing the likelihood of reaching a local min-

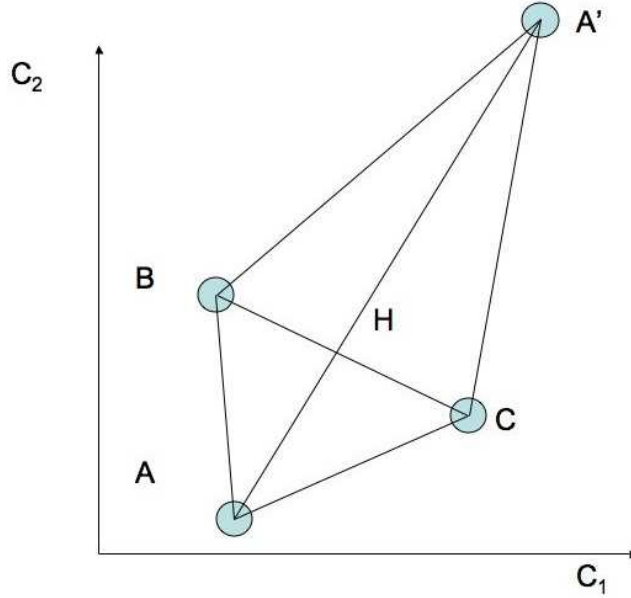


FIG. 7: (Color online) Expansion of the simplex

imum, the following steps were determined to be the most effective for finding the global minimum, when applying the above model to the snapshot data. The first one is to add an extra expansion when the original algorithm terminates: in case a value J_2 lower than the current minimum is found, the algorithm restarts. Once a minimum is attained, a 20×20 grid in the (C_1, C_2) plane is then created, each point being spaced by the termination tolerance. J_2 is evaluated at each of these points. If one of the 400 points in this local grid yields a lower value of J_2 than the current minimum, the algorithm is restarted at this point. The algorithm then terminates and returns the values of C_1 and C_2 that minimize J_2 . As a third and last step, we then restart this algorithm twice such that at each iteration we use the same initial search region and the current best guess of C_1 and C_2 as initial conditions. The new best estimates of C_1 and C_2 are then compared with the previous ones and it has been observed that 3 iterations are sufficient to obtain estimates within a few times the termination tolerances.

The estimation of C_1 and C_2 was performed using the modified NM algorithm to minimize the cost function J_2 . This cost function is however based on a spherical harmonics model for the fluxon distribution around the gyroscope, and the order of this expansion, conventionally denoted by the letter l , is in theory a free parameter. Nevertheless, early estimations and

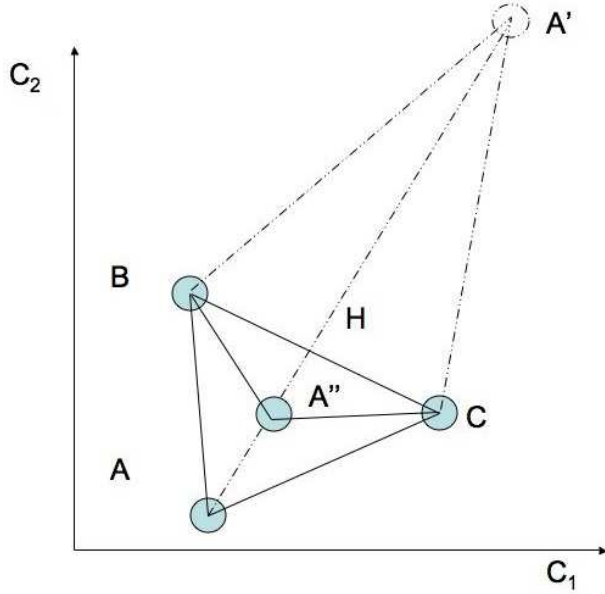


FIG. 8: (Color online) Simplex honing on a minimum : case $J_2(A') > J_2(A)$

fits to the SQUID data suggested a range of values for l . The NM search was thus repeated for all reasonable values of l . The optimal values for C_1 and C_2 were obtained by averaging the estimates corresponding to different values of l .

The standard deviation of the ensemble of estimates of C_1 and C_2 was on the order of 10 nHz for C_1 and 10^{-4} nHz/sec for C_2 . These results were obtained using one-day batches. Therefore, a conservative estimate of the uncertainty in $\dot{\phi}_s$ at the end of a one-day batch is: $10 \text{ nHz} + 10^{-4} \text{ nHz/sec} \times 86,400 \text{ sec} \approx 20 \text{ nHz}$ (see Eq. (15)). The uncertainty in the signal frequency, $f_z = \dot{\phi}_s/2\pi + f_p$, is then conservatively estimated to be 30 nHz, for a 10 nHz uncertainty in the polhode frequency, f_p . This uncertainty bounds the uncertainties for all gyroscopes during the entire science mission. For a gyroscope spinning at 60-80 Hz, this represents a relative error of 5×10^{-10} . Unlike the previous two approaches, the polhode motion of the gyroscopes is modeled explicitly. Therefore, the polhode frequency harmonics are completely separated from the gyroscope spin frequency estimates. The value of the signal frequency and decay rate for February 6th 2005 are given in tables III and IV. They can be compared with the results obtained with the phase differencing method on the same day in tables I and II.

gyro	signal frequency (Hz)
1	79.38746144
2	61.81765160
3	82.09121932
4	64.85036174

TABLE III: Signal frequency on February 6th 2005 at 07:39:00 GMT

gyro	frequency decay rate (nHz/sec)
1	0.1581
2	0.1432
3	0.3634
4	0.0803

TABLE IV: Signal frequency f_z decay rate on February 6th 2005

VII. CONCLUSION

This paper describes three successive algorithms for estimating the frequency of a digital signal. The first two of them, interpolated FFT and phase differencing, known previously, were properly adjusted for the needs of the analysis of the HF signal obtained in the Gravity Probe B experiment. The third method is new; it is based on the accuracy achieved by the previous two approaches, and involves a nonlinear estimation of a slowly changing frequency when many harmonics of another time-varying frequency are present. The last method requires accurately modeling the rigid body motion of a nearly torque-free gyroscope, and utilizes the specially modified Nelder-Mead simplex method.

These algorithms are applied to a particular problem of precisely determining the spin frequency of the ultra-precise GP-B gyroscopes. The measured HF SQUID signal was used for this analysis whose signal to noise ratio was $\sim 10^5$. We achieved the ultimate relative accuracy of 5 parts in 10^{10} , corresponding to the 30 nHz absolute accuracy for a gyro spinning at 60-80 Hz. This accuracy level was necessary for the estimation of trapped magnetic flux on the surface of each gyroscope rotor to 1%, the resulting time variations in the gyro readout

scale factor to 10^{-4} , and ultimately the relativistic gyro drift rate to 20 marcsec/yr.

- [1] G. E. Pugh, *WSEG Research Memorandum Number 111*, Weapons Systems Evaluation Group - The Pentagon, Washington D. C. - November 12, 1959.
- [2] L. I. Schiff, *Proc. Nat. Acad. Sci.* **46**, 871 (1960).
- [3] L. I. Schiff, *Phys. Rev. Lett.* **4**, 215 (1960).
- [4] R. Becker, G. Heller, F. Sauter, *Zeitschrift fur Physik* **85**, 772-787 (1933).
- [5] F. M. London, *Superfluids, Volume 1. Macroscopic Theory of Superconductivity* (Dover Publications Inc, Mineola, NY, 1961).
- [6] C. W. F. Everitt, D. B. DeBra, B. W. Parkinson, J. P. Turneure, J. W. Conklin, M. I. Heifetz, G. M. Keiser, A. S. Silbergleit, T. Holmes, J. Kolodziejczak, M. Al-Meshari, J. C. Mester, B. Muhlfelder, V. Solomonik, K. Stahl, P. Worden, W. Bencze, S. Buchman, B. Clarke, A. Al-Jadaan, H. Al-Jibreen, J. Li, J. A. Lipa, J. M. Lockhart, B. Al-Suwaidan, M. Taber, S. Wang, *Physical Review Letters* **106**, 221101-+ (2011).
- [7] A. Silbergleit, J. Conklin, D. DeBra, M. Dolphin, G. Keiser, J. Kozaczuk, D. Santiago, M. Salomon, P. Worden, *Space Science Reviews* **148**, 397-409 (2009).
- [8] J. Schoukens, R. Pintelon, H. Van Hamme, *Instrumentation and Measurement, IEEE Transactions on* **41**, 226-232 (1992).
- [9] G. S. Park, C. E. Cunningham, and B. Cabrera, *Physical Review Letters* **68**, 1920 (1992).
- [10] M. Salomon, Ph.D. thesis, Stanford University (2008).
- [11] D. C. Rife, G. A. Vincent, *Bell Syst. Tech. J* **49**, (2), 197-228 (1970).
- [12] G. M. Keiser and B. Cabrera, *Proceedings of the National Aerospace Meeting (Institute of Navigation Publications, Manassas, VA, 1982)*.
- [13] W. D. McMillan, *Dynamics of Rigid Bodies* (McGraw-Hill Book Company, Inc, New York, 1936).
- [14] J. A. Kozaczuk, *Precise Determination of Spin Speed and Spin Down-rate of Gravity Probe B Gyroscopes*, Stanford University Senior Honors Thesis (2007).
- [15] F. J. Harris, *Proceedings of the IEEE* **66**, 51 (IEEE Publications, New York, 1978).
- [16] A. V. Oppenheim and R. W. Schaffer, *Discrete-time signal processing* (Prentice-Hall, Upper Saddle River, NJ, 1999).

- [17] M. Avriel, *Nonlinear Programming: Analysis and Methods* (Dover Publications inc, Mineola, NY, 2003).